Study of the Thermal Stability of Hydrotalcite and Carbon Dioxide Capture Capacity of Hydrotalcite-derived Mixed Oxides using Molecular Dynamics Simulation

by

Muziyuan Gao

A thesis submitted in partial fulfillment of the requirements for the degree of

Master of Science

in

Materials Engineering

Department of Chemical and Materials Engineering
University of Alberta

Abstract

Hydrotalcites (HTlcs) or layered double hydroxides (LDHs) are used in a wide range of applications such as catalysis, electrochemical sensors, wastewater treatment and carbon dioxide (CO_2) capture. In this study, molecular dynamics simulation was employed to investigate carbon dioxide adsorption in amorphous layered double oxides (LDOs) derived from LDHs at elevated temperatures. The thermal stability of LDH was first examined by heating the sample up to T = 1700 K. Radial distribution functions confirmed the structural evolution upon heating and was in excellent agreement with experiments, where periclase was the main observed phase in the XRD patterns of the recrystallized mixed oxides above T = 1200 K. Further, CO_2 adsorption capacity was studied as a function of amorphous HTlc-derived oxide composition, where static and dynamic atomistic measures have been employed to characterize CO_2 capture capacity. We found that the CO_2 dynamic residence time on LDH-derived LDOs was sensitive to the Mg/Al molar ratio and CO_2 capture capacity reached maximum when the Mg/Al molar ratio was equal to 3.0. Meanwhile, the activation energy for diffusion also shows local maximum when the Mg/Al molar ratio is 3.0, suggesting that this particular ratio of Mg-Al mixed oxides possesses the highest CO_2 adsorption capacity and that it is consistent with experimental results. Examination of the binding between CO_2 and mixed oxides suggests that both magnesium and oxygen in amorphous LDOs contribute to CO_2 adsorption. Moreover, the effect of Mg-O and O (LDO)-C interaction are the most significant and the highest CO_2 adsorption capacity was observed in the system with the most Mg-O bindings and O (LDO)-C bindings.

Preface

Results presented in Chapter 3 and Chapter 4 of this thesis have been submitted for publication in the Journal of Physical Chemistry C entitled “Study of the Thermal Stability of Hydrotalcite and Carbon Dioxide Capture Capacity of Hydrotalcite-derived Mixed Oxides using Molecular Dynamics Simulation”.

For the work in the thesis, I was responsible for building computational models, performing simulations, analyzing data and composing manuscripts. Professor Hao Zhang and Professor Phillip Choi contributed to data analysis and manuscript revision. All of the researches are conducted under Professor Hao Zhang’s supervisions.

Acknowledgements

I gratefully appreciate guidance and encouragements of Dr. Hao Zhang and Dr. Phillip Choi during my graduate study.

I would like to thank the assistance from Mohammad Khalkhali, Xuhang Tong and Bin Liu in my research, also Seth Beck's revision of my paper.

I would like to thank my parents and Miss. Sijia Li for their supports.

Computational resources provided by WestGrid are appreciated.

Financial support from Canadian Centre for Clean Coal/Carbon and Mineral Processing Technologies (C^5MPT) is appreciated.

Table of Contents

List of Tables

List of Figures

List of Abbreviations

3D	three dimensional
BET	Brunauer–Emmett–Teller
GHGS	greenhouse gases
LDH	layered double hydroxide
LDO	layered double oxide
L-J	Lennard-Jones
MD	molecular dynamics
MSD	mean square displacement
PBC	periodic boundary condition
SPC	single point charge
RDF	radial distribution function
TSA	temperature swing adsorption
VDW	Van der Waals
VSA	vacuum swing adsorption
XRD	x-ray diffraction

1. Introduction

1.1 Layered double hydroxides

In the last few decades, there is growing consensus on global warming or climate change [1], and it is believed that one of the major causes is the anthropogenic greenhouse gases (GHGS) emission into the atmosphere. The combustion of fossil fuels that include coal, oil, lignite as well as natural gas produces carbon dioxide (CO_2), one of the major GHGS with high potential in industry engineering [2]. There are several options to reduce CO_2 emission into atmosphere [3]: 1) develop renewable energy for the substitution of fossil fuels; 2) increase the burning efficiency of fossil fuels, which could reduce the cost of the industry; 3) capture CO_2 prior to emission into the atmosphere. Due to the low cost of fossil fuels, it is difficult to find renewable energy to replace it, and that is why it is crucial to reduce CO_2 emission [4]. The CO_2 capture and separation have been divided into three main categories [5]: post-combustion processes for tradition coal-fired power plants, pre-combustion processes for gasification and oxy-fuel combustion. Considering economic cost, technical limitations, CO_2 capture and separation in fossil fueled plants has been proposed crucial to investigate as a result of awareness of climate change [6]. Among various techniques used for the removal of CO_2 from burning fossil fuel, such as pressure swing adsorption (PSA) [3], vacuum swing adsorption (VSA), and temperature swing adsorption (TSA), the PSA process is conducted as the most suitable option because the process can be operated at elevated temperatures so that no more

energy is required for cooing fuel to ambient temperature prior to CO_2 emission. However, it is imperative to find appropriate CO_2 adsorbent as the PSA is processed at elevated temperature, and the thermal stability of adsorbents should be guaranteed. In addition, other properties of the CO_2 adsorbent are also required: 1) sufficient kinetics for CO_2 adsorption under operating conditions [7]; 2) efficient stability upon CO_2 adsorption cycle; 3) adequate hydrothermal and mechanical stability. Pre-combustion CO_2 capture is one of the CO_2 capture and storage (CCS) technologies that involve separating CO_2 from hydrogen-rich shift gas from sweet/sour water-gas shift reactors. Successful commercialization of the above technologies relies on high-performance, reversible solid CO_2 adsorbents with a sufficiently high CO_2 adsorption capacity at elevated temperatures and fast adsorption and desorption kinetics.

In recent years, several research groups have developed potential solid sorbents for CO_2 capture because they are cost-effective compared with that of the aqueous amine-based sorbents. The solid CO_2 sorbents have been divided into three major categories according to their working temperatures: low temperature sorbent (< 473 K) [8], such as carbon-based sorbent, zeolites-based sorbent; intermediate temperature sorbent (473 - 673 K) [9-11], such as layered double hydroxides (LDHs), MgO-based sorbent; high temperature sorbent (> 673 K) [12-15], such as CaO-based sorbent, silicate-based sorbent. Among various solid CO_2 adsorbents, LDHs have been recognized as one of the most suitable materials for carbon dioxide adsorption in intermediate temperature range, which consist of positively charged brucite-like layers with interlayer space containing charge-compensating anions, illustrated in Fig.1.1 [16].

The general formula for LDHs is $[M^{II}_{1-x}M^{III}_{x}(OH)_2]^{x+}\ A^{n-}_{x/n} \bullet mH_2O$, where M^{II} is divalent cation (e.g., Mg^{2+}), some of which are substituted by trivalent cation M^{III} (e.g., Al^{3+}), and A is an anion (e.g., OH^-, CO_3^{2-}, Cl^-, NO_3^-), where x is normally in the range of 0.2-0.4 [8][17].

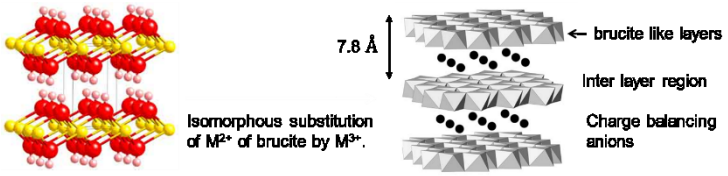

Brucite LDH

Figure 1.1 The structure of layered double hydroxide based on brucite [16].

Due to the availability of LDHs as naturally occurring minerals or synthesized LDHs as bulk quantities with relatively low cost [18], there is a growing interest on their characteristics scientifically. With a range of trivalent and divalent cationic combinations available in LDHs, the cationic ratio can be modified within a wide range. Furthermore, any anions can be intercalated into the inter layer region between brucite-like layers, which indicate LDHs possess large anion exchange capacity. The LDHs have not only been applied into CO_2 adsorption, but used as catalysis, polymer nanocomposites, and ion exchangers as well [19].

1.2 Structural changes of layered double hydroxides

The structural changes of LDHs during thermal treatment have been experimentally investigated in the previous studies. Yang et al. performed a study by in situ techniques for thermal evolution of Mg-Al LDHs, illustrated in Fig.1.2 [20], and they suggested that Mg-Al LDH first dehydrated between 343 K and 463 K while the

remaining was the layered structure; then dehydroxylated and transformed into an amorphous phase between 463 K and 678 K, and finally lost anions in the temperature range of 678 - 853 K, where X-ray diffraction peaks showed spinel ($MgAl_2O_4$) and brucite (MgO) formed, which contributed to CO_2 capture [21].

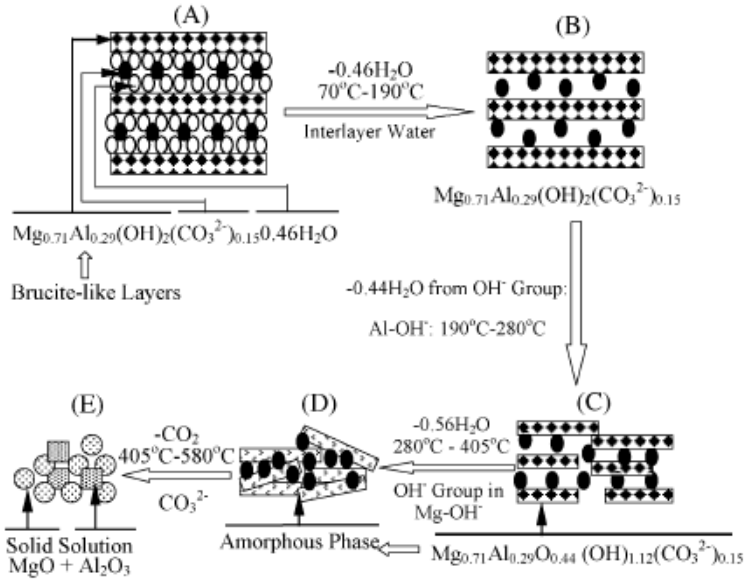

Figure 1.2 Structural changes of layered double hydroxide during thermal evolution. The temperature changes from 343 K to 853 K [20].

Borau.et.al. [22] also synthesized an Mg/Al layered double hydroxide (LDH) using the coprecipitation method. The synthesized LDH and its calcination products were characterized by X-ray diffraction illustrated in Fig.1.3. The XRD pattern of the LDH at room temperature exhibited common features of layered materials: strong peaks at low 2θ values and weaker peaks at high 2θ values. Structural changes produced by calcination of the LDHs samples at 473 K showed no significant changes in the structures. On the other hand, the LDH structure collapsed at a calcination temperature of 773 K and a periclase (MgO) phase formed, which was consistent with

previous findings that pericalse was the main phase at this calcination temperature. With raising temperature to 1073 K, there were no changes in the phase. Finally, sharp reflections for spinel ($MgAl_2O_4$) appeared and the MgO peaks became more significant.

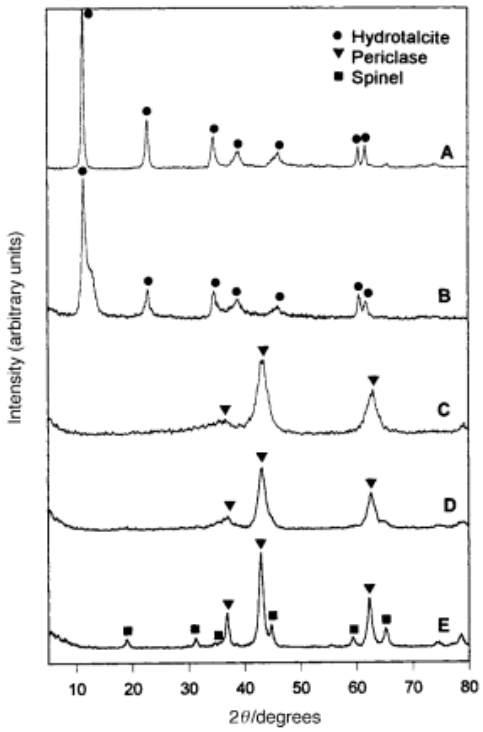

Figure 1.3 XRD patterns for HT-Mg/Al at room temperature (A) and its products of calcination at 473 K (B), 773 K (C), 1073 K (D) and 1273 K (E) [22]

1.3 CO_2 adsorption of LDHs-derived oxides

Although LDHs have been identified as one of the most suitable materials within the range of 473-673 K [3][23], it is well accepted that the LDH itself does not possess appreciable CO_2 capture capacity because of limited room between layers. Recently, many studies have been published on the CO_2 adsorption of LDH-derived adsorbents. Wang et al. [24] systematically investigated a series of Mg-M-CO_3 LDHs (M=Al, Fe,

Ga, Mn) and demonstrated that different phases form upon heating and M^{3+} determined the CO_2 adsorption capacity and they also suggested the maximum CO_2 capture capacity at 673 K of quasi-amorphous LDHs. Hutson et al. [19] subsequently identified that both physical and chemical CO_2 adsorption of Mg_3Al_1-LDH increased with pressure. They also showed that Mg_3Al_1Cl LDH possessed the highest physisorption/chemisorption ratio, while $Mg_3Al_1CO_3$ LDH had the highest combined CO_2 adsorption. Reddy et al. [25] also found that Mg-Al-CO_3 had the highest CO_2 capture capacity after calcined at around 673 K, and it was confirmed by Gao et al [26] who suggested that there existed an optimum temperature for CO_2 capture of LDHs-derived mixed oxides as the spinel ($MgAl_2O_4$). A stable oxide structure would form when the temperature was high enough so that Mg and Al would react with each other in mixed oxides. The temperature cannot be too low because thermal energy has to be high enough to break Mg-OH and Al-OH bonds so that the hydroxides can be completely removed. A further study by Gao et al. [26] for the effect of Mg/Al ratio on CO_2 capture capacity of amorphous mixed oxide at 673 K demonstrated CO_2 capture capacity was highest when the Mg/Al molar ratio was between 3.0 and 3.5. Evidently, the Mg/Al ratio is a key parameter that determines the surface characteristics of the LDH-derived mixed oxides. However, Sharma [27] investigated the CO_2 capture capacity on a series of Mg-Al-CO_3 LDH samples with varied Mg/Al ratio parameters, and concluded that 37% Al content (Mg/Al molar ratio is 1.7) was the optimal condition for CO_2 adsorption at 303 K and 333 K. It is noted their experiments were performed in different temperature regions. Nevertheless, the previous studies suggest

that the Mg/Al molar ratio is a key parameter determining the CO_2 adsorption capacity of the LDH-derived mixed oxides.

Recent studies suggested that CO_2 uptake capacity of LDH-derived mixed oxides changed with increasing temperature. Marta et al. [28] found a decrease in CO_2 uptake of Mg-Al-CO_3 LDH-derived mixed oxide as the adsorption temperature increased from 323 k to 373 K. Moreover, different adsorption sites exhibit different CO_2 adsorption capacity. Majority of adsorption sites correspond to physisorption and some are chemisorption sites. As a result, the available surface area is also an important factor [29]. Bolognini [30] introduced Brunauer–Emmett–Teller (BET) surface area to investigate multilayer CO_2 adsorption of Mg-Al mixed oxides. They found that the number of medium strength sites, which was predominate for CO_2 adsorption when Mg/Al molar ratio was between 2.0 and 3.5, was closely related to Mg^{2+}-O^{2-} and Al^{3+}-O^{2-} pairs. A latter study by Bellotto [31] also characterized the structure of Mg-Al mixed oxides with a regular close-packed oxygen cubic. However, due to the strong difference of bond distance between Mg-O and Al-O, the cations were not distributed with a long-range order instead Mg^{2+} is in octahedral and Al^{3+} is in tetrahedral coordination when the Mg/Al ratio is 2.0.

1.4 Aims of molecular dynamics simulation

Experimental understanding of the molecular-level origin of the complex structure and CO_2 adsorption mechanisms on LDHs and LDHs-derived mixed oxides is usually difficult because of the limitation of conventional experimental techniques. However, molecular modeling on the other hand has been highly successful over the last decade

in filling this gap and providing better molecular-level understanding. Kirkpatrick and colleagues investigated the structural and energetic origins of LDH compounds containing short chain carboxylic acids using computational molecular dynamics (MD) study. [32][33] The hydrated interlayer galleries were found to be stabilized by an integrated hydrogen-bonding network among the anions, water molecules and hydroxyl groups of the LDH layers. [34] Zhao and Burns investigated benzene sorption mechanisms intercalated into interlayers of organoclays, which were synthesized from single chain quaternary ammonium cations (QAC), using MD modelling and proposed a model to predict the QAC–clay microstructures. [35] These studies have demonstrated the utility of MD methods to investigate the structure aspects of organic clay composites and provided significant insights. In atomistic modeling, we employ empirical potential (force field) to describe interatomic interaction between molecules and atoms. We hope to predict the materials properties that have not been used in the fitting of force field. In order to confirm the prediction, the simulation results need to be compared with the available experimental results. Clays and related layered minerals are fine grained and poorly crystalline materials and MD simulations have become extremely helpful in providing an atomistic perspective on the structure and behavior of clay minerals. Randall.et.al. [36] developed empirical force fields that has been previously used to describe the interatomic interactions for clay and hydroxide and presented CLAYFF force field. CLAYFF force field is based on the single point charge (SPC) water model [37], and it can accurately describe the bulk structures of a wide range of hydroxide phases.

1.5 Objectives of this study

The main objective of this study is to investigate the thermal stability of Mg-Al-Cl layered double hydroxides and capacity of CO_2 capture in LDHs-derived oxides using molecular dynamics simulations. The objectives of this research are further divided into the following aspects:

1) The structural changes of LDHs during thermal evolution are directly related to the temperature. The Mg-Al-Cl LDH sample when the Mg/Al ratio is 3.0 is processed, and the structural changes of LDH during thermal evolution from 300K and 1700K will be characterized utilizing radial distribution function (RDF) and X-ray diffraction (XRD). The objective of this study is to better understand the structural evolution upon heating from the perspective of atomic level.

2) We will characterize the atomic structure of amorphous LDH derived mixed oxides as a function of composition, which could be directly related to the CO_2 capture capacity.

3) The static and dynamics of CO_2 adsorption are to be conducted in MD simulation to investigate the distribution behavior and strength of CO_2 adsorption of amorphous LDOs to understand the adsorption mechanisms and correlation with structure. A series of Mg-Al-Cl LDH samples with a different Mg/Al ratio (1.7:1; 2.2:1; 3.0:1; 3.7:1) are processed, and further quantitative analysis of the CO_2 adsorption behaviors could explain the relationship between capacity of CO_2 adsorption and the Mg/Al molar ratio.

2. Simulation details

With great effort made in the last several decades, molecular dynamics simulation has become a powerful tool to investigate the structures and properties of various materials. Given the interatomic potentials (force fields), MD could provide in-depth insights into the structural behaviors of layered double hydroxides; especially those phenomena that are hardly characterized using experimental methods. For instance, MD could provide direct access to energy states, atomic local stress, and atomic trajectories, which help determine the static and dynamic properties of amorphous LDOs.

2.1 Principle of MD simulation

Molecular dynamics simulation is based on Newton's second law of motion:

$$\overrightarrow{F_i} = m_i \overrightarrow{a_i} \quad (1)$$

Where $\overrightarrow{F_i}$, m_i and $\overrightarrow{a_i}$ are the force, mass and acceleration of atom i, respectively. Integration of the equation of each atom yields the trajectories, i.e., positions, velocities and accelerations of each atom as a function of time. To start a typical simulation, the inputs are potential, initial positions and velocities of each atom in the system for MD simulation.

The acting force on each atom is derived from the interatomic potential energy as a function of their positions as follows:

$$\overrightarrow{F_i} = -\nabla V(r_i) \quad (2)$$

where V represents interatomic potential energy, r_i represents the i atom's position. Combining equations (1) and (2), we obtain:

$$-\nabla V(r_i) \equiv m_i \left(\frac{\partial^2 r_{ix}}{\partial t^2}, \frac{\partial^2 r_{iy}}{\partial t^2}, \frac{\partial^2 r_{iz}}{\partial t^2}\right) \quad (3)$$

As shown in equation (3), the initial conditions are important to conduct a MD simulation. Each of them would exert an influence on the trajectories of simulations, especially the interatomic potential energy V as the accurate choice of V would directly determine the reliability of simulation results. More information on potentials will be given in the next section.

The following schematic graph shows a typical process of MD simulation.

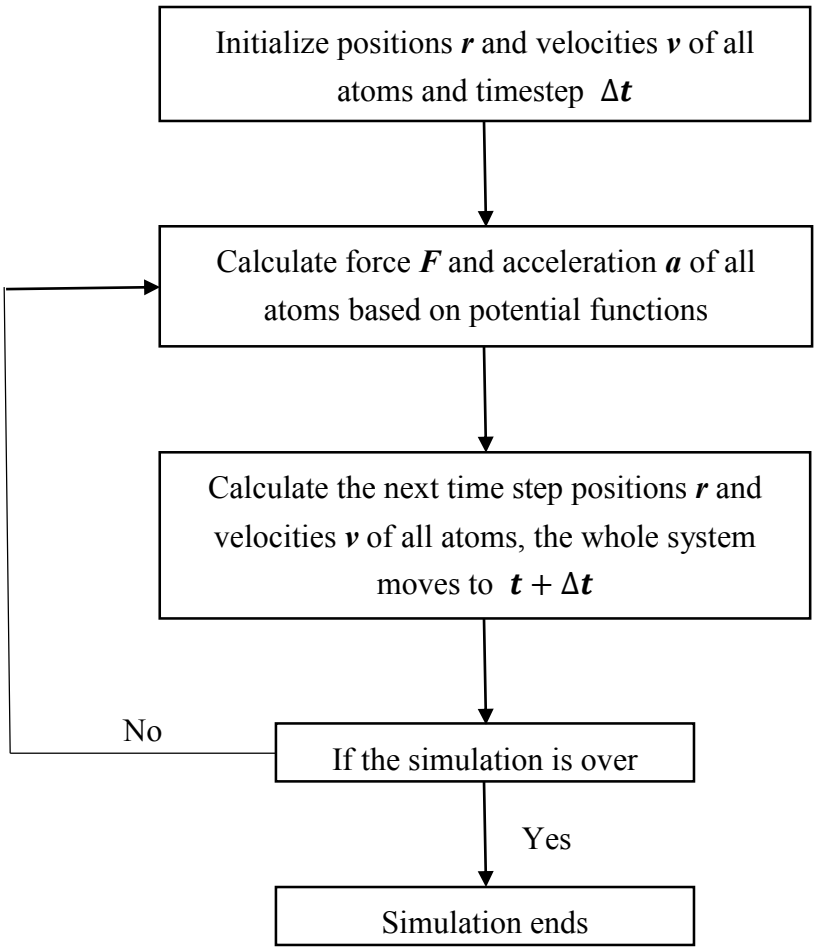

Figure 2.1 Schematic representation of MD simulation

The simulation loops through alternatively calculating forces and accelerations obtained from new positions. In practice, MD codes not only have to integrate the equation of motion but also calculate temperature, pressure etc. Moreover, the ensemble chosen in MD simulation, as well as the targets of simulation, should also be considered. As mentioned above, a few key components such as potential, integration algorithm, temperature, pressure deserve detailed elaboration, which would be introduced in the following sections.

2.2 Force field parameters

Any atomistic simulations depend on the accuracy of the description of atomics interactions. The most accurate description may be provided by the first-principle method based on quantum-mechanical treatment of electrons. Unfortunately, this accurate description used to describe the inter-atomic interactions, also limits the systems' sizes in first-principle simulations, although some allow the degrees of freedom associated with swelling and lateral displacement of the lattice. Moreover, quantum mechanical methods based on density functional theory are computationally expensive and cannot handle large number of atoms, although results are more accurate. [36]

Teppen et al. [38] developed a new force field based on a rigorous analysis from quantum mechanics calculations. Bonded interaction terms were used to simulate clay phases successfully, and the use of O-Al-O angle bend potential to treat both tetrahedrally and octahedrally coordinated aluminum atoms was a predominant progress as there was no published force fields that could evaluate the effect of octahedral coordination before. The zeolite-based force fields were subsequently developed and applied into application which included tetrahedral aluminum only. [39-42] Bougeard et al. [43] also developed an empirical force field of kaolinite which made all of the atoms free to translate but limited to small scale simulations of relatively well-known mineral structures, because large number of force field parameters are required to describe the bonded states. Sainz-Diaz et al [44] then developed a force field, in which three-body bond bend terms were added to

guarantee metal-oxygen coordination, and it performed well in describing the structures of various medium and high charge phyllosilicates. However, it was not adaptable for low charge phases such as pyrophyllite where weak interactions occur.

Randall et al [36] presented an alternative approach to solve the transferability issue of atoms for MD simulations of hydrated crystalline compounds. Based on nonbonded description of the metal-oxygen interactions related to hydrated phases, the CLAYFF force field used an empirically derived interaction parameters which described the potential energy between atoms in layered structure of LDH accurately [45][46]. However, current empirical force fields could not provide an accurate description of the interactions between CO_2 and oxides successfully. Although three-site models for CO_2 are compatible with CLAYFF force field, they lack bond flexibility of CO_2 so that the vibrational behavior of both the gaseous and liquid CO_2 cannot be examined. Zhu [47] simplified the three-site model of CO_2 that was compatible with CLAYFF force field, and developed a fully flexible model for CO_2 that allowed intramolecular bond stretch and angle bend. As a result, it improved the accuracy of interfacial simulations between liquids and solids. Randall [48] then optimized the force field parameters in order to improve the accuracy of symmetrical bond stretch frequency. The total potential energy of the system can be calculated as

$$U_{total} = U_{intermolecular} + U_{intramolecular} \quad (4)$$

Equation (5) and (6) provides the expression of intermolecular and intramolecular energy in terms of contributing energy terms.

$$U_{intermolecular} = E_{VDW} + E_{Coul} \quad (5)$$

$$U_{intramolecular} = E_{stretch} + E_{bend} \quad (6)$$

The Van der Waals and Coulombic energy contribute to the nonbonded energy of system. No dielectric medium presented is assumed to evaluate the interaction for short-range Van der Waals energy described by pair wise-additive Lennard-Jones (L-J) 12-6 potentials [49], which is given by equation (7). The Coulombic energy reveals the electric interaction between atoms, and it can be calculated as equation (8).

$$U_{VDW}(r_{ij}) = 4\varepsilon_{ij}\left[\left(\frac{\sigma_{ij}}{r_{ij}}\right)^{12} - \left(\frac{\sigma_{ij}}{\sigma_{ij}}\right)^{6}\right] \quad (7)$$

$$U_{Coul}(r_{ij}) = \frac{q_i q_j}{4\pi\varepsilon_0 r_{ij}} \quad (8)$$

Where ε_{ij}, σ_{ij} are L-J well depth and L-J size, respectively, q_i, q_j and r_{ij} are the partial charges of atoms and distance between atom i and atom j; ε_0 is the permittivity of free space. The intramolecular part consists of bond stretching and bond angle vibration. Harmonic potentials [50] are used for the bond stretch and angle bend terms calculated by equation (9).

$$U_{intramolecular} = \frac{1}{2}k_r(r - r_0)^2 + \frac{1}{2}k_\theta(\theta - \theta_0)^2 \quad (9)$$

Where r, r_0 are the bending bond length, θ and θ_0 are the bending angle, and k_r, k_θ are the force constant.

In this study, both non-bonded (van der Waals and Coulombic) and bonded (bond, angle, torsion and improper) interactions have been applied. The atom type for Mg and Al are octahedral magnesium (mgo) and octahedral aluminum (ao). Oxygen

partial charges vary from -0.95 for hydroxyl oxygen (oh), to -1.1808 for bridging oxygen with octahedral substitution (obos) [36]. Aqueous chloride ion (Cl) with a partial charge of -1.0 has been intercalated into the inter layer region for charge balancing. Moreover, partial charge of carbon dioxide on amorphous surface of mixed oxides was modified based on previous research [48]. Combined with potential parameters in CLAYFF [36], we could evaluate the Van der Waals interaction between CO_2 and the surface of amorphous LDOs. All the force field parameters used in this study are listed in Table 2.1 and Table 2.2.

Table 2.1 Nonbond parameters for the CLAYFF Force Field

species	charge (e)	D_0 (kcal/mol)	R (Å)
octahedral magnesium	1.3600	9.0298×10^{-7}	5.2643
octahedral aluminum	1.5750	1.3298×10^{-6}	4.2713
hydroxyl oxygen	-0.9500	0.1554	3.1655
bridging oxygen with octahedral substitution	-1.1808	0.1554	3.1655
aqueous chloride ion	-1.0	0.1001	4.3999
C in CO_2	0.6512	0.0559	2.800
O in CO_2	-0.3256	0.1597	3.028

Table 2.2 Bond and angle parameters for CO_2

bond stretch			
species i	species j	k_1(kcal/mol · Å)	r_0(Å)
C	O	2018	1.162

angle bend				
species i	species j	species k	k_2(kcal/mol.rad^2)	θ_0(deg)
O	C	O	108.0	180

2.3 Simulation configuration

An atomic configuration of the simulation cell of Mg_3Al_1-LDH, containing chlorine intercalated into inter layer region for charge balancing, was shown in Fig.2.2. The simulation cell consisted of 4465 atoms with a dimension of approximately 3.7 nm × 6.4 nm × 2.3 nm in X, Y and Z directions, respectively. Molecular dynamic simulations were performed in the constant composition, isothermal-isobaric (NPT) ensemble to investigate the structural changes of the LDH at 300K. In MD simulations, periodic boundary conditions were applied in three dimensions. Pressure was maintained based on Parrinello-Rahman method [51], where zero pressure was employed in the X, Y and Z direction and constant temperature (T) was controlled by the Nose-Hoover method [52-53]. After initial construction of the model, energy minimization was conducted until the force and energy tolerance were under 10^{-5}

kcal/(mol · Å) and 10^{-7} kcal/mol. In this study, continuous heating was processed from 300 K to 800 K with a heating rate of 2.5×10^{11} K/s to investigate the transformation from LDH to amorphous LDO. After the layered structure of LDH collapsed at 800 K, all the anions, hydrogen and some of the oxygen atoms were removed from the system. After maintaining the structure at 900K extended time for structure equilibrium, the amorphous LDOs were then heated up to 2000 K at the same heating rate to investigate the thermal evolution of amorphous LDOs. As specific kinetic processes cannot be observed under continuous temperature change, isothermal heating for an extended period of time is required. We performed simulation for two nanoseconds with time step of 1 femtosecond, and atom configurations were dumped every 2000 time steps (2 picoseconds) for data storage and analysis in isothermal heating. To have a comprehensive understanding of thermal evolution of LDH, isothermal simulations were employed at specific temperatures: T = 300 K, 700 K, 800 K, 900 K, 1200 K and 1700 K.

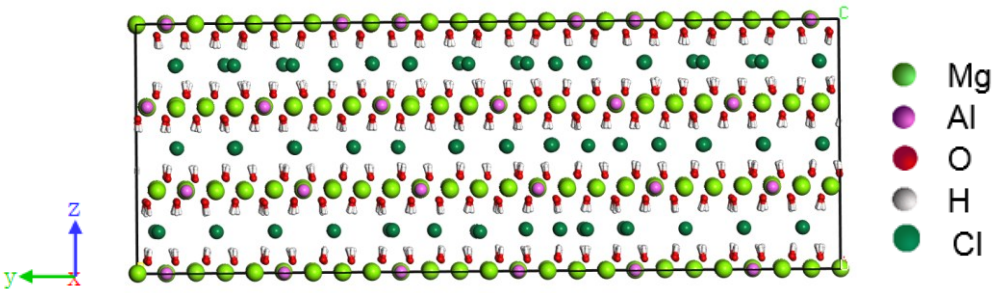

Figure 2.2 Equilibrated structure of LDH model from molecular dynamics simulation using NPT ensemble at 300 K.

2.4 CO_2 adsorption simulations of amorphous LDOs

At 900 K, all the anions and hydroxyl disappeared and LDH transformed to amorphous LDO (Mg-Al mixed oxide). Gutierrez et al. [54] found that the Al^{3+} ions of amorphous Al_2O_3 were mainly tetrahedral at high temperature, as well as present shorter bond length and lower fraction of octahedrally coordinated Al compared to crystal structure. Continually cooling amorphous LDO from 900 K to 300 K with a cooling rate of 2.0×10^{11} K/s with total time of 2 ns was employed through NPT ensemble. In order to study the CO_2 adsorption on amorphous LDO, CO_2 molecules were first added into the vacuum gap above the surface of amorphous LDO according to corresponding pressure, which could be calculated by Van der Waals equation of state [55]. Molecular dynamic simulations were applied using a canonical ensemble to investigate the CO_2 adsorption of amorphous LDO at 300 K. MD simulations were performed for 2 ns and atom configurations were also dumped every 2 ps for data analysis in isothermal cooling. Fig.2.3 shows the distribution of multilayered CO_2 molecules arranged along the x×z plane of amorphous LDO.

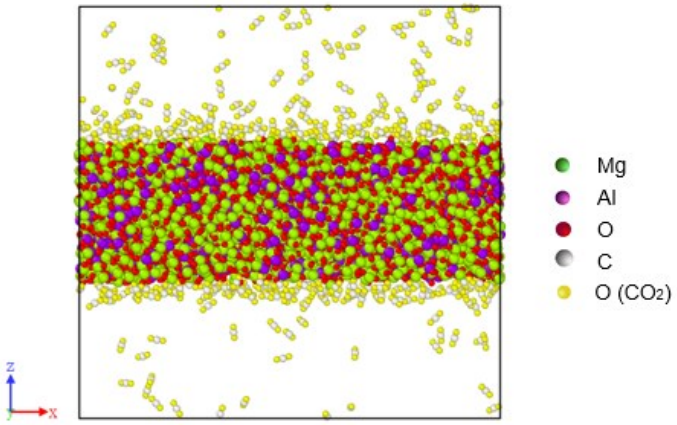

Figure 2.3 Structure of amorphous LDO when Mg/Al molar ratio is 3.0 with multilayered CO_2 adsorption on the surface. Molecular dynamics simulation was done in NVT ensemble at 300 K

2.5 Simulation package

Classical molecular dynamics simulations were performed to characterize the thermal evolution of LDH and CO_2 adsorption of LDH-derived mixed oxide, which was carried out in LAMMPS [56], developed at the Sandia National Laboratories. Voronoi tessellation has been applied to investigate the coordination number of atoms in the simulation cell. The two-dimensional definition of a Voronoi diagram is a partitioning of a plane into regions based on distance to points in a specific subset of the plane. For each set of points (called seeds, sites, or generators) there is a corresponding region consisting of all points closer to that seed than to any other, and the region is called a Voronoi cell [57]. The definition of Voronoi tessellation in three dimensions is similar to two dimensions, Although the simulation cell is three dimensional, the theory of Voronoi tessellation is similar with two dimensions and the number of edges of a Voronoi cell is equal to the coordination number.

2.6 Summary

Molecular dynamics is a powerful tool for investigating the structural changes of LDH and CO_2 adsorption of LDH-derived mixed oxide. In MD, the length scale could reach up to hundreds of nanometers and the time scale could reach up to several nanoseconds. By employing this technique, we could study the atomic behaviors of LDH and have a further study of the microscopic structure of LDH-derived mixed oxide. In current study, we built a full 3D simulation cell by Materials Studio, then covert it to the formats that can be used in LAMMPS. With the help of Ovito [58], the structural changes of the system with increasing temperature can be visualized and the dynamic CO_2 behaviors can be clearly revealed as well.

To ensure the accuracy of the information extracted from MD simulations, the following aspects need to be carefully considered. The first issue is the efficiency of the interatomic potential, because all the simulation results are determined by the potential. The simplified CLAYFF force field developed by Randall is proven suitable to simulate the CO_2 behaviors. The second issue is the limited time scale in MD simulation. As the simulation time is limited to a few ns, a typical heating or cooling rate in MD simulation is around 2.0 to 2.5×10^{11} K/s, which is several orders of magnitude greater than in experimental studies. Thus, the atom configurations need to be carefully verified, especially for isothermal processes.

3. Thermal evolution of LDH[1]

The Mg/Al molar ratio of Mg-Al-LDHs plays crucial roles in determining the CO_2 adsorption capacity of LDHs and LDHs-derived mixed oxides. To have a clear understanding of the transformation process from Mg-Al-LDH to mixed oxides, Mg_3Al_1-LDH is assumed to be applied in our research. The anion intercalated into interlayer region for charge balancing is also a key parameter to investigate the thermal evolution of Mg_3Al_1-LDHs. Various theoretical methods have been applied to compare CO_2 adsorption between different intercalated anions, such as Mg_3Al_1-Cl LDHs and Mg_3Al_1-CO_3 LDHs. Although the Mg_3Al_1-CO_3 LDHs possess remarkable CO_2 capture capacity, the ratio of physisorption/chemisorption is not as high as Mg_3Al_1-Cl LDHs. What is more, the CVFF force field [59] is required to applied for CO_3^{2-} as CLAYFF force field parameters are not adaptable to CO_3^{2-}. As a result, the layered structure of LDHs is not stable due to the abnormal charge interaction between CO_3^{2-} and brucite-like layer of LDHs. Therefore, we choose Cl ion to balance the charge. Objectives of this study are to investigate 1) the collapse of layered structure of LDH during thermal evolution between 300 K and 900 K; 2) energy and structure changes of LDH-derived amorphous LDO from 900 K to 1700 K; 3) structure and composition of amorphous LDO at 300 K.

To achieve the objectives, we first employed the MD simulation to study the

[1] The results presented in this chapter have been submitted for publication in the Journal of Physical Chemistry C.

thermal evolution of Mg_3Al_1Cl-LDH with increasing temperature between 300 K and 900 K, and shed light on the structural changes from LDH to amorphous LDO. Then we would reveal the structure and composition of amorphous LDO including bond distance change between metal ion and oxygen and atom distribution density as a function of distance.

3.1 Simulation configuration

The crystal unit cell of Mg_3Al_1Cl-LDH is built up as R-3m with x, y dimension is equal to 33.138 Å, and z dimension of 23.4 Å by materials studio. The detailed atom geometric information after intercalating anions into inter layer region is provided in Table 3.1. The unit cell was modified as rectangular coordinate, and Al was substituted into the layered structure of LDH for Mg randomly. We could adjust the Mg/Al molar ratio by increasing Al substitution, and Cl^- was then intercalated into inter layer region for charge balancing.

Table 3.1 Atom geometric information of crystal structure unit

Atom	Site	x/a	y/b	z/c
Mg	3a	0	0	0
O	6c	1/3	2/3	0.0407
H	6c	1/3	2/3	0.0822

The lattice of unit cell was shown in Fig.3.1. Since the periodic boundary condition is applied to all X, Y and Z directions, the unit can be expanded to 6×6 supercell as

shown in Fig.2.2.

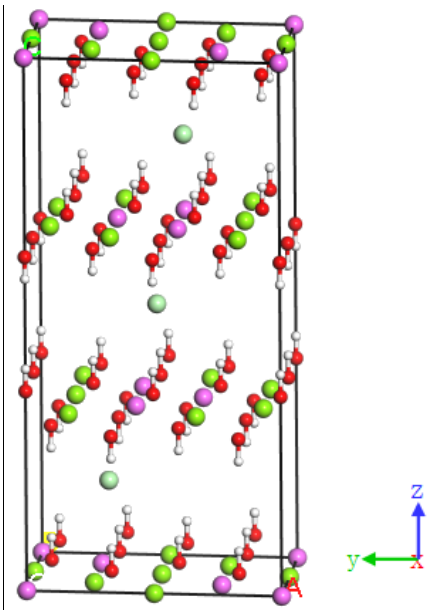

Figure 3.1 The unit cell of Mg_3Al_1Cl-LDHs built up as rectangular coordinate.

All simulations were conducted with LAMMPS [48]. Atomic potential energy with increasing temperature was dumped every 1 ps. Simulated atomic configurations were visualized by Ovito [58]. Atomic distribution density was revealed by Radial Distribution Function (RDF). Atomic coordination number was calculated using Voronoi tessellation [57]

3.2 Results and discussion

3.2.1 Structural changes of LDH upon heating

Fig.3.2 shows the potential energy ($E_{potential}$) change with increasing temperature up to 900 K and there is an abrupt jump at 800K, which indicates the layered structure of LDH has begun to collapse and transformed to LDO. Radial distribution function (RDF) was carried out to investigate the thermal evolution of

Mg-Al-Cl LDH, which helps uncover the structural changes during thermal treatment. The inset in Fig.3.2 shows the RDF of Mg-Al-Cl LDH (Mg/Al=3) from 300 K to 800 K. The RDF at 300 K shows a typical pattern of crystalline structure including a sharp peak centered at ~2.1 Å and other peaks at other interatomic distance. The RDFs do not exhibit significant changes with increasing temperature from 300 K to 700 K, which indicates that the Mg-Al-LDH retains its layered crystalline structure. However, the RDF at 800 K shows typical features of a liquid, suggesting that the original crystalline structure turns into an amorphous structure at about 800 K.

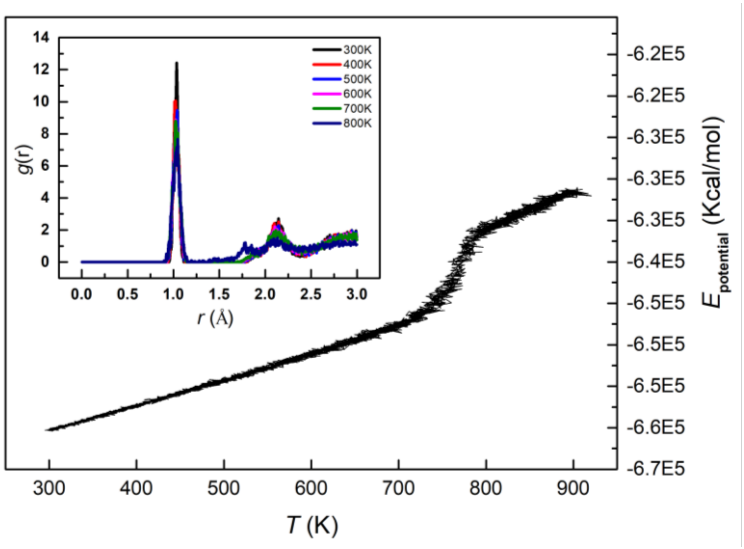

Figure 3.2 The temperature dependence of potential energy of Mg-Al-Cl-LDH with a Mg/Al ratio of 3.0 over the temperature range of 300 K – 900 K. The inset shows the corresponding radial distribution function g(r) of Mg-Al-Cl-LDH during thermal evolution between 300 K and 800 K.

When temperature was higher than 700K, LDH began to dehydroxylate and bonds between atoms were gradually broken. Fig.3.3 supports such observation as the average

bond distance of O-H, and Mg-O increase abruptly when temperature is higher than 700K, which suggests the binding between O and H is weaken and magnesium oxide is transformed from a crystalline structure into amorphous structure. The results are consistent with the bond distance in layered mineral brucite $Mg(OH)_2$ calculated by Philippe et al. [60]. In general, crystal phases have higher density than liquids, as well as shorter average bond lengths. However, Gutierrez et al. [54] investigated the structural properties of liquid Al_2O_3 in a molecular dynamics study and demonstrated that the liquid phase of Al_2O_3 was indeed denser than the crystal phase and possessed larger fraction of tetrahedral coordinated Al. In addition, in the current study, the Al atoms substitutes Mg atoms in the LDHs structure, causing the Al-O bond length in LDHs is much longer than that in Al_2O_3 crystal. Hence, we should expect a drop in Al-O bond length as the structure transfers to amorphous state. As shown in Fig.3.3, the average bond distance of Al-O indeed had an abrupt drop when the temperature was higher than 700K.

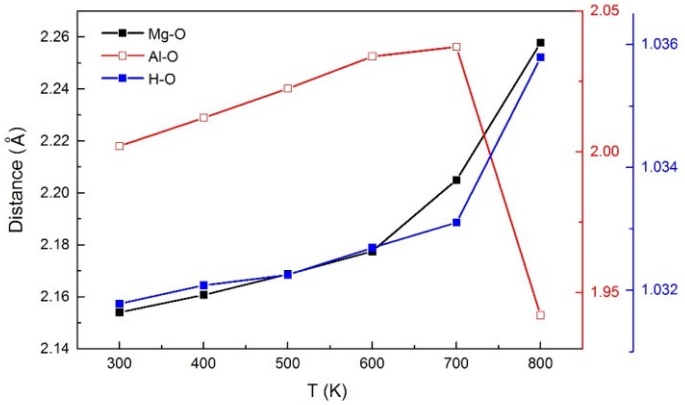

Figure 3.3 Mg-O, Al-O and O-H distance variance during thermal evolution of LDH from 300 K to 800 K

After the layer structure of LDHs collapsed, we removed hydroxyl and anions and then continued to maintain the system at 900 K for 2 ns to form LDOs. Fig3.4 shows the change in potential energy of LDOs by increasing the temperature from 800 K to 1700 K. With increasing temperature, the potential energy of amorphous LDOs continuously increased between 800 K and 1700 K. However, there existed an abrupt drop at 1200 K, which manifested another phase transformation. The sharp jump in potential energy around 1700 K suggests a first-order phase transformation, in which the LDOs melt to liquid phase. RDF diagrams in the inset of Figure 3.4 shows typical amorphous structure with two broad peaks centered at 2 Å and 2.8 Å at 900 K. This indicates that LDH transforms to an amorphous structure. However, the RDF at 1200 K shows four distinct broad peaks centered on ~ 2 Å, 3 Å, 4.8 Å and 6.6 Å, indicating the emerging crystalline structure of LDOs. The RDF at 1700 K indicates that the structure has transformed back to amorphous (i.e., melting of the LDOs).

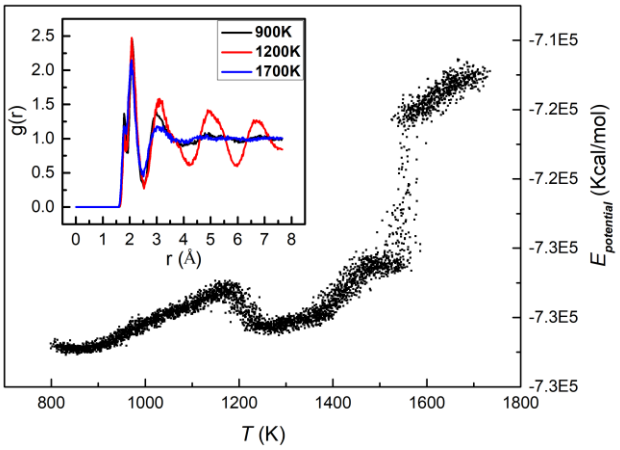

Figure 3.4 The potential energy as a function of temperature of amorphous LDO. The inset shows radial distribution function, g(r) of Mg-Al-Cl-LDH during thermal evolution between 800 K and 1700 K.

3.2.2 Structure and composition of amorphous LDO

To further examine the structural evolution of LDH, XRD patterns were calculated at different temperatures. Figure 3.5 summaries these patterns that indicate that the thermal evolution involves three stages. In the first stage, which is from 300 K to 700 K, XRD patterns show sharp peaks that imply there is no significant change of layered structure in LDH. The XRD pattern of LDH from simulation indeed agrees very well with experimental observations [61]. However, layered structure of LDH began to collapse and transformed into amorphous structure at 800 K (the second stage) as no obvious peaks appeared. With further temperature increase, two broad peaks centered at $2\theta \approx 30°$ and $2\theta \approx 60°$ at 900 K manifesting amorphous LDOs formed. The two peaks centered at $2\theta \approx 42.8°$ and $62.0°– 62.4°$ at 1200 K indicate amorphous LDOs recrystallized. This is in agreement with previous observations [22][62], which

indicates that periclase (MgO) was the main observed phase in Mg_3Al_1-LDH derived mixed oxides. In the third stage, crystalline LDOs melted to liquid and returned to amorphous structure again at 1700 K.

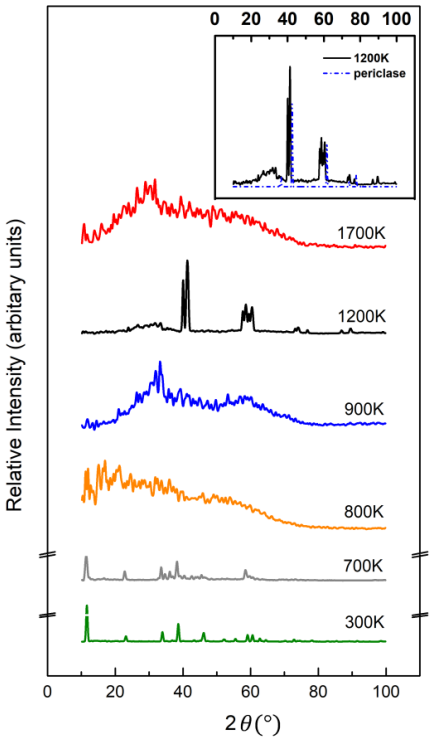

Figure 3.5 XRD patterns of LDHs from 300 K to 1700 K. The inset shows comparison between XRD of LDOs structure and experimental periclase at 1200 K.

We cooled down the structure of amorphous LDO from 900 K to 300 K with a cooling rate of 2×10^{11} K/s. The structure of amorphous LDO is maintained at 300 K for additional simulation of 2 ns to reach equilibrium. The atomic configuration of amorphous LDO is illustrated in Fig.3.6 (a). In order to reveal the structure of amorphous LDO at 300K, detailed information of each atom, especially the coordination number of atoms in the simulation cells was characterized. In this study, Voronoi tessellation has been applied to calculate the coordination number of

magnesium atoms in different Mg/Al molar ratios, as shown in Fig.3.6 (b). The coordination number of magnesium atoms is close to 6 when the Mg/Al molar ratio is 3.0, which means every magnesium atom is surrounded by 6 atoms on average. Whereas the coordination number of magnesium atoms is close to 5 when the Mg/Al molar ratio is other than 3.0, as the fraction is close to 100 percent for Mg/Al molar ratios are 1.7 and 2.2 and near 70 percent for Mg/Al molar ratio is 3.7. In other words, the coordination number of magnesium atoms is highest when the Mg/Al molar ratio is 3.0 in four different Mg/Al molar ratios. The inset shows the probability of finding oxygen in Mg^{2+} in four different molar ratios. Most magnesium atoms are surrounded by five-oxygen when the Mg/Al molar ratio is 3.0. However, most magnesium atoms are surrounded by four-oxygen when the molar ratio is 1.7, 2.2 and 3.7. It can be concluded that the structures of amorphous LDO at 300K are different in four Mg/Al molar ratios and the magnesium atoms of amorphous LDO are inclined to bind with more atoms, especially oxygen when the Mg/Al molar ratio is 3.0.

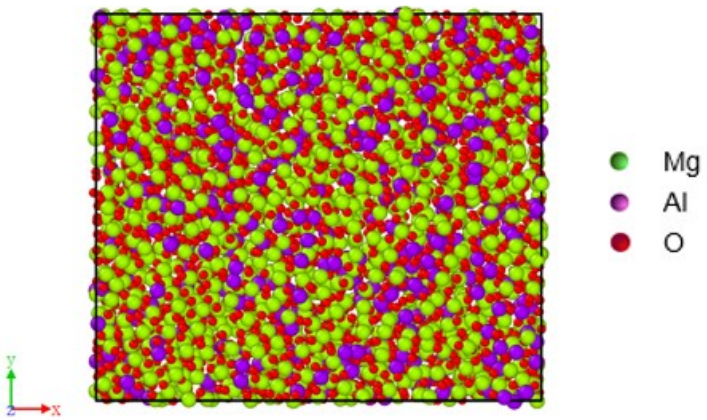

(a)

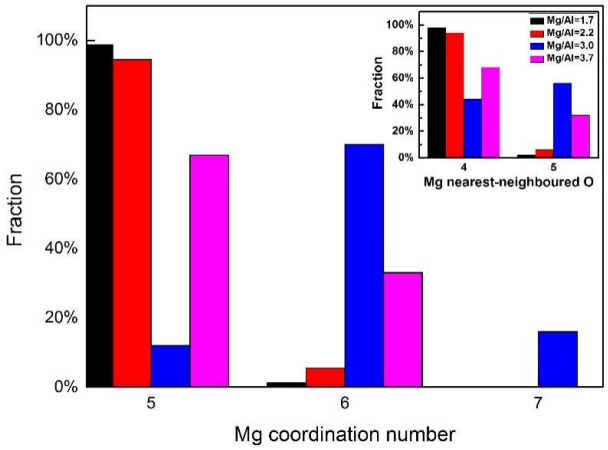

(b)

Figure 3.6 (a) An atomic configuration of amorphous LDOs viewed in x×y plane at 300 K. (b) The coordination number of magnesium atoms at different Mg/Al molar ratios. The inset shows the fraction of oxygen occupation in coordination number of magnesium.

4. CO_2 adsorption of amorphous LDOs[2]

To clarify CO_2 adsorption mechanisms on the surface of amorphous LDOs, we conducted a molecular dynamics simulation study. In this study, the measurement of CO_2 adsorption has been investigated through two approaches, i.e., "the static adsorption" and "the dynamic adsorption". The "static adsorption" measures the amount of CO_2 molecules accumulated near the surface. Whereas, the "dynamic adsorption" reveals the CO_2 adsorption behavior including trapped into the surface or moving randomly in the vacuum above the surface. The main objective of this study is to investigate effects of atoms on the surface of amorphous LDO on strength and durance of CO_2 adsorption capacity in different Mg/Al molar ratios.

4.1 Simulation details

To examine CO_2 adsorption capacity as a function of amorphous composition, four different Mg/Al ratio models were built, i.e., Mg/Al=1.7, 2.2, 3.0, and 3.7. We cooled amorphous LDO in four different ratios from 900 K to 300 K, and created vacuum gap above the two free surfaces of amorphous LDO. The CO_2 capture capacity of LDH-derived amorphous LDO was investigated at the room temperature. As Youssef [63] found, increasing pressure had a positive effect on CO_2 adsorption of

[2] The results presented in this chapter have been submitted for publication in the Journal of Physical Chemistry C.

MCM-41 silica at ambient temperature multilayer CO_2 adsorption. In order to study the static CO_2 adsorption of amorphous LDO, CO_2 molecules were added into the vacuum gap above the surface of amorphous LDO according to corresponding pressure. The Van der Waals equation of state [55] was applied to evaluate the amount of CO_2 molecules in the simulation cell above the surface of amorphous LDO,

$$\left[P + a\left(\frac{n}{v}\right)^2\right]\left(\frac{v}{n} - b\right) = RT \qquad (10)$$

where a and b are constants; n is number of moles; and P, V, T are pressure, volume and temperature for a real gas, respectively.

A series of NPT were performed to confirm the agreement between the pressure calculated from experimentally developed Van der Waals equation of state and the one obtained from molecule dynamics simulations [64]. MD simulations were applied using isothermal-isobaric (NPT) ensemble via Nose-Hoover thermostat [52][53] to investigate the CO_2 adsorption on the surface of amorphous LDO at 300 K. The initially constructed system was relaxed at 900 K for 2000 ps (the time interval is 1 fs). The model system was then cooled to 300 K at a cooling rate of 2.0×10^{11} K/s before CO_2 have been added into the vacuum above the surface of amorphous LDO. During the cooling progress, pressures in X, Y and Z directions were controlled at 0 bar. After above-mentioned cooling, MD simulations were applied using a canonical NVT ensemble to investigate the CO_2 adsorption of amorphous LDO at 300 K. Systems were visualized using Ovito [58]. All simulations were carried out in the Lattice provided by WestGrid.

In order to study the structure and composition of amorphous LDO, partial RDF [65] has been used to describe the binding between atoms on the surface of amorphous LDO and the first CO_2 adsorption layer, and the integrated partial RDF is related to the coordination number on the surface of amorphous LDO in four different Mg/Al molar ratios.

4.2 Results

4.2.1 Static CO_2 adsorption

The static adsorption describes describes how the local density of CO_2 molecules varies as a function of distance from the surface of amorphous LDOs. Figure 4.1 shows the CO_2 density profile in contact with amorphous LDOs with different Mg/Al molar ratios. The middle section in Figure 4.1 represents the bulk amorphous LDOs and therefore, the density of CO_2 is zero in this region. The four different samples exhibit similar CO_2 distribution behaviour, where two broad peaks centered at -2.5 and 26 Å and the broad peak width is about 9 Å. This means that most of the CO_2 molecules were adsorbed within 9 Å regime above the surface, whereas, the remaining CO2 distributed in the vacuum. The orientation of the CO_2 molecules in the first adsorption layer in four different Mg/Al molar ratios is also shown in Figure 4.2. Since CO_2 is a linear molecule, the orientation is defined as the angle between CO_2 molecular axis and normal to the amorphous LDO's surface, and the most probable angle is 90°. In other words, CO_2 molecules in the first adsorption layer are mainly horizontal with respect to the surface of amorphous LDO.

The static CO_2 adsorption measure shows the overall adsorption behaviour of CO_2 on the LDOs' surfaces. In addition, it provides the information of a length scale, i.e., thickness of the adsorbed CO_2 layer. The overall adsorption behaviours of different Mg/Al molar ratios show no significant difference. This is probably due to the fact that the static adsorption is a time-average measurement, while the adsorption behaviour itself is a dynamic process; therefore, additional dynamic analysis is needed to seek the difference affected by the composition of the amorphous LDOs.

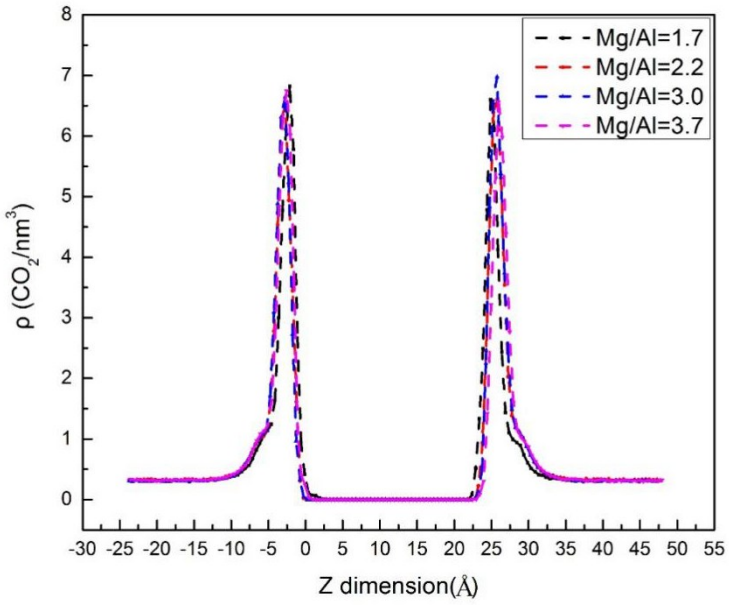

Figure 4.1 Density distribution of adsorbed CO_2 at four different Mg/Al ratios: 1.7, 2.2, 3.0, and 3.7.

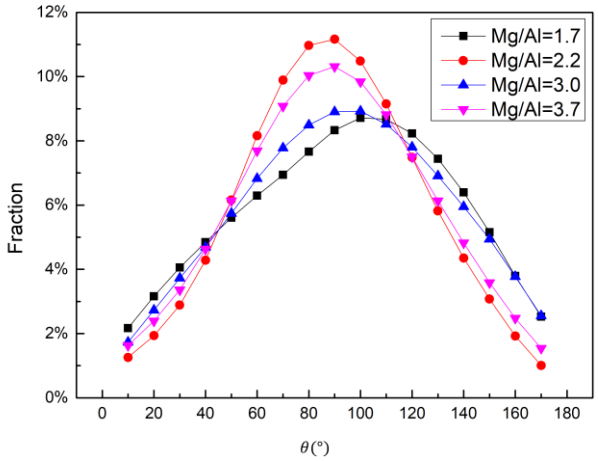

Figure 4.2 Orientation of CO_2 molecules within the first adsorption layer calculated for the system with P = 60 atm. Orientation is defined as the angle between the molecular axis of CO_2 molecules and normal to the amorphous LDO surface.

4.2.2 Dynamic CO_2 adsorption

For dynamic CO_2 adsorption, we used the definition proposed by Impey et al [66], which was first employed to calculate the residence time of water molecules and has been used extensively to study the hydration behavior of ions, surfaces and nanostructures [67]. Following our previous work [64], we used a simplified version of this quantity defined as

$$\tau_i(t) = \sum < P_i(t_0, t) > \cdot \Delta t \qquad (11)$$

where $\tau_i(t)$ is the i^{th} CO_2 residence time within distance criteria for adsorption at t, $P_i(t_0, t)$ is a parameter of the i^{th} CO_2 molecule which takes values 0 or 1. $P_i(t_0, t)$ equals to 1 if a CO_2 molecule is marked as adsorbed on the surface of amorphous LDO at t_0 and t, and it has not left out of the specific distance for any continuous period between t_0 and t. Under other circumstances, it takes a value of 0. Δt is the time step at which the observation is made to check adsorption of the i^{th} CO_2.

In this definition, t_0 is updated if a CO_2 molecule leaves the adsorption layer and comes back to it. This means that each CO_2 molecule has multiple residence times, and we can calculate the number of adsorbed CO_2 within a specific time window. Figure 4.3 shows the typical semi-log plot of residence time versus amount of adsorbed CO_2 for amorphous LDO with Mg/Al = 3.0.

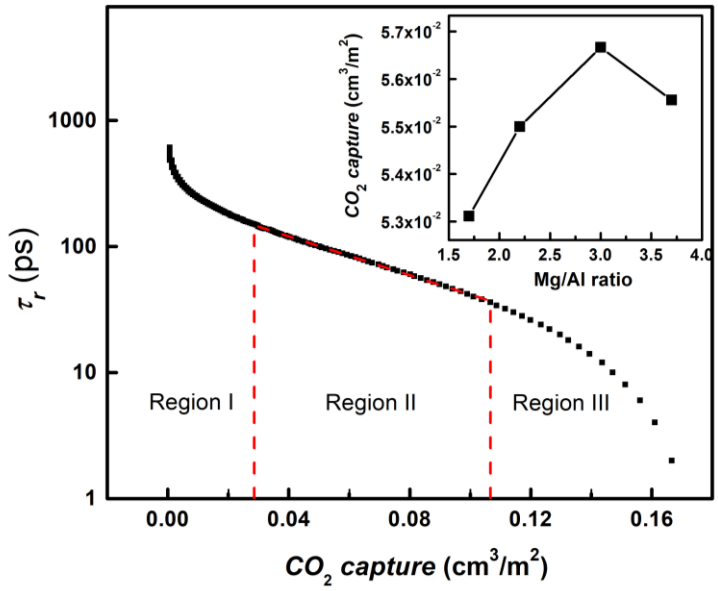

Figure 4.3 Residence time of adsorbed CO_2 with amount of adsorbed CO_2. The inset shows the adsorption capacity as a function of LDO compositions.

Previous study suggests that individual CO_2 molecules reside near the defects on the surface for extended time, and majority CO_2 molecules dynamically visit and leave the surface, which makes the residence time of CO_2 a dynamic value. A cut-off distance of 9 Å has been used to define a CO_2 molecule as adsorbed on the surface for all four samples with different Mg/Al ratios. This value is chosen according to density profile of CO_2 molecules near the oxide surface, as suggested by Figure 4.1 using static adsorption measurement. In Figure 4.3, we show a typical residence time versus the

amount of adsorbed CO_2 molecules of Mg_3Al_1-LDH derived LDO. Because CO_2 molecules behave rather differently as distance varies from the surface of amorphous LDO, three distinctive regions can be recognized in the residence time diagram of CO_2 molecules. In region I, there are a few number of CO_2 molecules with relatively long residence times for more than 600 picoseconds. In region III, CO_2 molecules visit the adsorption layer with high frequency but stay in this layer for short periods of time. None of these two regions in the semi-log plot shows linear relationship. In region II, the residence time versus amount of CO_2 in semi-log plot follows linear relationship; phenomenologically, we can express the residence time as follows.

$$\tau_r \sim e^{-\frac{n}{<n>}} \tag{12}$$

where, τ_r represents the residence time, n is the number of adsorbed molecules, and <n> the average number of molecules adsorbed on the surface. We believe the region II represents the steady-state adsorption behaviour of CO2 on the surface.

In the present study, all four compositions possess similar relationships between residence time and CO_2 adsorption. In order to compare CO_2 adsorption between different Mg/Al molar ratios, the number of adsorbed CO_2 during the second stage was rescaled by the surface area of each composition, as shown in the inset of Figure 4.3. The figure clearly shows that the dynamic adsorption of CO_2 molecules on the LDH-derived amorphous LDO is sensitive to Mg/Al molar ratio. Overall, with increasing Al content, CO_2 adsorption increases, and the CO_2 capture capacity reaches maximum when Mg/Al molar ratio is equal to 3.0. Gao et al. [26] also investigated the

effect of Mg/Al molar ratio on CO_2 adsorption at high temperatures, and their experimental results agreed well with current simulation observations. It is worth to mention that the CO_2 adsorption units in this study are different from experimental ones, because current CO_2 capture capacity is only dependent on the area of two free surfaces, while the total volume of the adsorbent can be arbitrarily changed by changing the dimension along z-axis. In order words, the BET surface area of amorphous LDO is the predominant parameter for CO_2 adsorption, and that is why the CO_2 adsorption should be rescaled by the surface area of each composition. The CO_2 adsorption simulation at high temperatures obviously deserves further investigation.

4.2.3 CO_2 diffusion

The other related dynamic property of CO_2 adsorption is the diffusion of CO_2 molecules on the surface. The mean squared displacement (MSD) analysis of CO_2 was performed by computing the square of the displacements of all CO_2 molecules [68] within a specified time interval Δt. The MSD was defined as

$$MSD = \frac{1}{N}\sum_{n=1}^{N} |r_n(t_0 + \Delta t) - r_n(t_0)|^2 \qquad (13)$$

where N is the total number of atoms, and $r(t_0)$ is the position of the atom at t_0. The MSD of carbon dioxide was calculated at five difference temperatures from 273 K to 375 K for each composition and three representative MSD for Mg/Al molar ratio of 3.0 are shown in Figure 4.4 (a). The slope of MSD versus time intervals is proportional

to the diffusion efficient D [69], and the temperature dependence of the diffusion coefficients can be well approximately by

$$D = D_0 e^{-\frac{Q}{RT}} \tag{14}$$

Where D_0 is pre-exponential factor, and Q is the activation energy for diffusion. Figure 4.4 (b) shows the Arrhenius temperature dependence of diffusion coefficients and the slopes yield the activation energy for diffusion. The activation energy for diffusion obtained in current study falls into the same ballpark of previous studies [70-72]. The inset shows the activation energy of CO_2 diffusion as a function of LDO composition and it suggests that Mg/Al molar ratio is 3.0 possesses highest diffusion barrier. That result is consistent with observation that dynamic CO_2 capture capacity of Mg/Al molar ratio = 3.0 is highest (see inset of Figure 4.3).

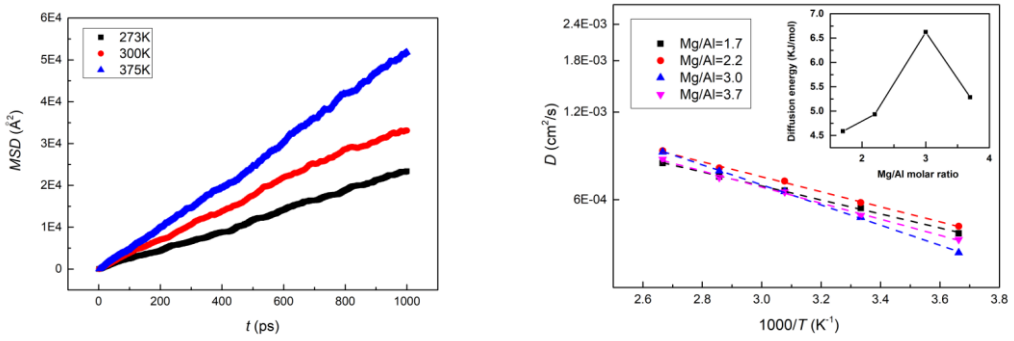

(a) (b)

Figure 4.4 (a) Mean square displacement versus time in different temperatures: 273 K, 300 K, and 375 K when the Mg/Al molar ratio is 3.0. (b) Arrhenius temperature dependence of diffusion coefficient for four different Mg/Al molar ratios: 1.7, 2.2, 3.0, and 3.7. The inset shows the diffusion activation energy as a function of Mg/Al molar ratio.

4.2.4 Partial radial distribution function of amorphous LDO

Both the dynamic adsorption and diffusion coefficient data point to the direction that the Mg/Al molar ratio of 3.0 possesses the highest CO_2 capture capacity. How does this dynamic property relate to amorphous structure? We further investigated the binding arrangement between CO_2 molecules and amorphous LDO to reveal the potential correlation. Bolognini [30] demonstrated that the chemical reaction between CO_2 and Mg^{2+}-O^{2-} or Al^{3+}-O^{2-} pairs was a key parameter for CO_2 adsorption, and Yong [73] concluded that increasing aluminum content strongly affected CO_2 adsorption because of larger charge of Al. Unfortunately, in MD simulation we can only observe physisorption. In my current study, only Mg-O, Al-O and O (LDO)-C binding lengths were studied as ions that had the same signs with repulsive Columbic interaction did not contribute in binding and the radial distribution function (RDF) of atoms has been normalized as follows [65]:

$$\mathrm{g}(r) = \lim_{dr \to 0} \frac{p(r)}{4\pi(N_{pairs}/v)r^2 dr} \tag{15}$$

$$\mathrm{g}^*(r) = \mathrm{g}(r) * N_{Pairs} \tag{16}$$

where r is the distance between a pair of atoms, $p(r)$ is the average number of atom pairs at a distance between r and $r + dr$, V is the total volume of the simulation cell, and N_{pairs} is the number of unique pairs of atoms where one atom is from each of two selections. In current case, the N_{pairs} of partial RDF is the product of number of magnesium, aluminum or oxygen atoms on the surface and oxygen or carbon atoms of CO_2 molecules.

Figure 4.5 (a) (b) (c) (d) show the rescaled partial RDF of atoms on the surface of amorphous LDO with different Mg/Al molar ratios. The pair RDF of Al-O indicates that the binding length of Al-O is longest, suggesting that aluminum atoms on the surface of amorphous LDOs possess weak interaction with the first layer of CO_2 molecules. It is also noticed that the binding length of Mg-O is shortest, which indicates that magnesium atoms on the amorphous surface are mainly bound with the first CO_2 adsorption layer. The Figure 4.6 shows the integrated $g^*(r)$ of Mg^{2+}, which is related to the coordination number on the surface, in amorphous LDO with four different Mg/Al molar ratio: 1.7, 2.2, 3.0 and 3.7. It reveals that the binding between Mg^{2+} and the first CO_2 adsorption layer is relatively high for Mg/Al molar ratio = 3.0. This is also related to the fact that the Mg^{2+} in the bulk amorphous LDO with a Mg/Al molar ratio of 3.0 has higher coordination number and on the surface they tender to bind with more atoms, as suggested in Figure 3.6 (b).

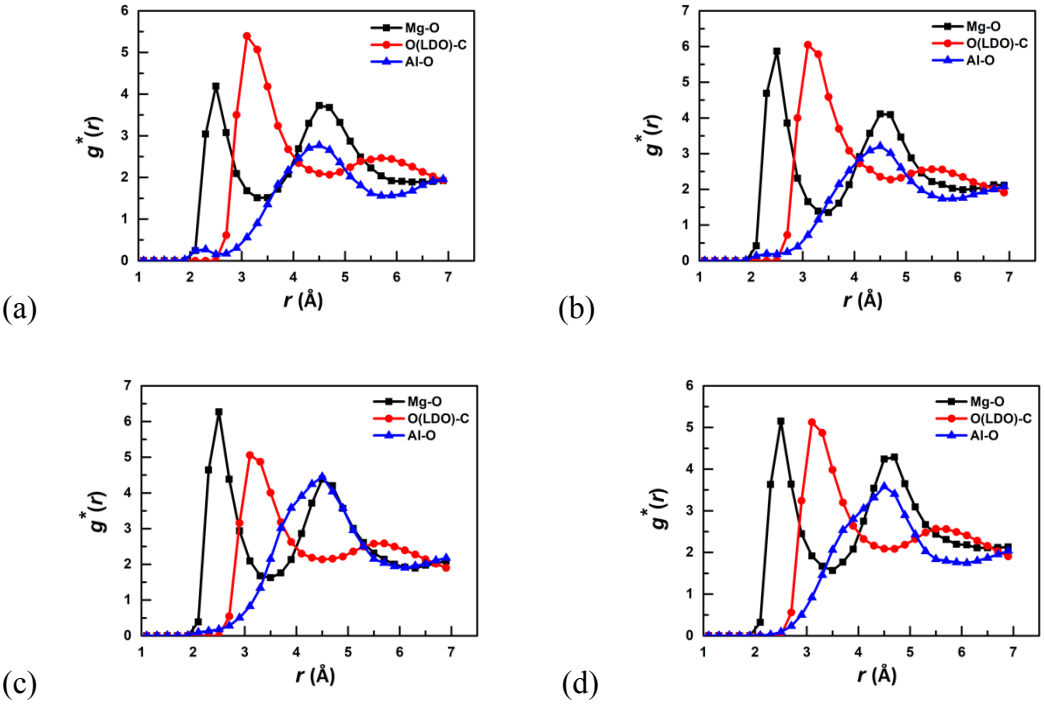

Figure 4.5 Partial RDF of CO_2 and amorphous LDO: (a) Mg/Al molar ratio of 1.7 (b) Mg/Al molar ratio of 2.2, (c) Mg/Al molar ratio of 3.0, and (d) Mg/Al molar ratio of 3.7. Mg-O and Al-O represent the respective binding arrangement between CO_2 and magnesium and aluminum atoms in the amorphous LDO, O(LDO)-C represents the binding arrangement between CO_2 and oxygen atoms in the amorphous LDO.

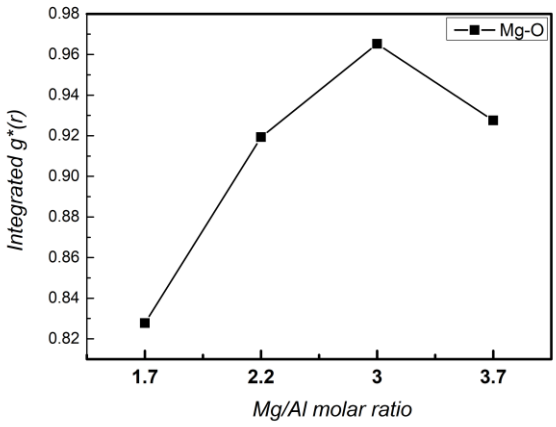

Figure 4.6 Integrated partial RDF of Mg^{2+} in amorphous LDO in four different Mg/Al molar ratios: 1.7, 2.2, 3.0, and 3.7.

4.3 Discussion

In this study, we further investigated the binding arrangement between CO_2 molecules and amorphous LDO to reveal the potential correlation. Figure 4.7 shows the binding arrangement between atoms on the surface of amorphous LDO and the first layer of adsorbed CO_2 molecules in four different Mg/Al molar ratios. Only heterocharged atoms of amorphous LDO are considered, such as Mg^{2+}-O, Al^{3+}-O, O^{2-}-C, because homocharged atoms will possess repulsive interaction between CO_2 molecules and amorphous LDO. It implies that the binding between Mg^{2+} on the surface and the first CO_2 adsorption layer is predominant, whereas, the binding fraction of Al-O is minor, which corresponds to the results of partial RDF. In addition, the fraction of binding between Mg^{2+} and CO_2 is relatively high for Mg/Al molar ratio = 3.0. This also corresponds to the conclusion that the Mg^{2+} in Mg/Al molar ratio = 3.0 tends to bind with more atoms.

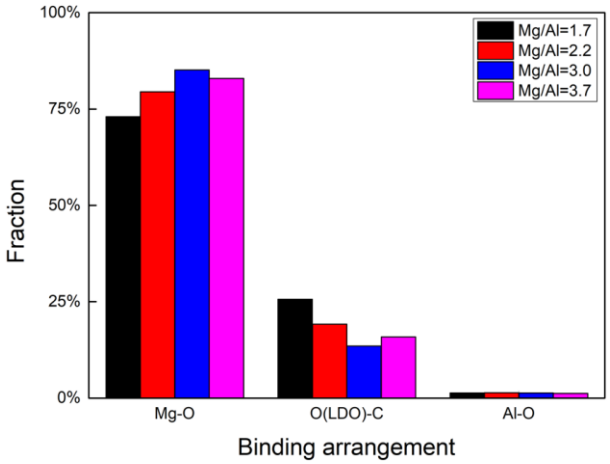

Figure 4.7 Binding fraction between CO_2 molecules and amorphous LDO. Mg-O represents the binding between Mg^{2+} and oxygen atoms of CO_2; O (LDO)-C represents binding between O^{2-} of amorphous LDO and carbon atoms of CO_2; Al-O represents binding between Al^{3+} of amorphous LDO and oxygen atoms of CO_2.

4.4 Summary

In summary, we investigated the effect of Mg/Al molar ratio parameter of LDH-derived oxide on their CO_2 adsorption capacity. We have shown similar static CO_2 adsorption and an overall longer residence time near the surface of amorphous LDO in different Mg/Al molar ratios. However, the CO_2 molecules in different molar ratios shows distinctive dynamic residence times, which reveals that their CO_2 adsorption strengths are different. In order to study their CO_2 adsorption behaviors, the angle orientation of CO_2 molecules near the surface of amorphous LDO has been investigated. We find the adsorbed CO_2 molecules are mainly horizontal to the surface of amorphous LDO, and they are primarily adsorbed within 9 Å through Mg-O interaction. To verify the origin that Mg^{2+} act as CO_2 adsorption sites, partial RDF of

atoms on the surface of amorphous LDO and binding fraction between CO_2 and amorphous LDO are done. We find that the binding between Mg^{2+} and O^{2-} in CO_2 molecules is strongest in all four different Mg/Al molar ratios, and the CO_2 capture capacity is highest when Mg/Al molar ratio is 3.0 due to high fraction of Mg-O binding.

5. Conclusions

5.1 Conclusions

In this work, molecular dynamics simulations were employed to investigate the 1) structural changes of LDH during thermal evolution; 2) the structure and composition of amorphous LDO and 3) CO_2 adsorption of amorphous LDOs. The following are three main conclusions drawn from this thesis study:

1) The thermal evolution of Mg_3Al_1Cl LDH has been investigated under NPT ensemble. The layered structure begins to collapse and hydroxyl groups and anions are removed at 800 K, where LDH transforms to amorphous LDO. However, amorphous LDO recrystallizes at 1200 K and retains crystal structure between 1200 K and 1600 K. Moreover, the crystal structure of LDO at 1200K is close to periclase. With increasing temperature, LDO melts to liquid phase at 1700 K, and returns to amorphous structure again.
2) Molecular dynamics simulation is employed to study the structure and composition of amorphous LDO at 300 K. When the Mg/Al molar ratio is 3.0, the coordination number of magnesium atoms is close to 6, which is highest in the four different ratios. Moreover, the occupation fraction of oxygen of most magnesium atoms is 5, and it is also highest in the four different ratios. It can be concluded that the structures of amorphous LDO at 300 K are different in four Mg/Al molar ratios and the magnesium atoms of amorphous LDO are inclined to bind with more atoms, especially oxygen when the Mg/Al molar ratio is 3.0.

3) The CO_2 adsorption of amorphous LDOs has been studied from two aspects: 1) the static CO_2 adsorption and 2) the dynamic CO_2 adsorption. The static CO_2 adsorption shows the overall adsorption behavior of CO_2 molecules above the amorphous LDO surface. It is found that the four different samples exhibit similar CO_2 distribution behaviors. Most CO_2 molecules accumulate near the surface and are adsorbed within 9 Å above the surface, whereas, the remaining CO_2 molecules distributed in the vacuum. CO_2 molecules dynamically visit and leave the surface of amorphous LDO, and three different CO_2 residence time has been observed: 1) particular CO_2 molecules reside on the surface of amorphous LDO for relatively long time; 2) the CO_2 far away from the surface visit the surface of amorphous LDO for very short time; 3) the remaining CO_2, whose residence time versus amount of CO_2 in semi-log plot follows linear relationship, reside on the surface for relatively long time. The dynamic CO_2 adsorption in the four different Mg/Al molar ratios possess similar relationship, and the capacity of CO_2 adsorption reaches maximum when Mg/Al molar ratio is 3.0, which agrees well with previous experimental CO_2 adsorption of amorphous LDO at high temperature [26]. Moreover, the activation energy of CO_2 for diffusion as a function of LDO composition also suggests that a higher CO_2 diffusion barrier is required when the Mg/Al molar ratio is 3.0, which is consistent with the dynamic CO_2 adsorption results. The CO_2 capture capacity of amorphous LDOs is also the most favorable at the same molar ratio, which is in agreement with previous experimental studies. The partial RDF of atoms on

the surface of amorphous LDO proves that magnesium atoms contribute to the first CO_2 capture layer. The binding arrangement between CO_2 molecules and amorphous LDO's surface indicates that the binding between magnesium and oxygen predominant in the first layer of CO_2 adsorption. A relatively higher integrated $g^*(r)$ of Mg-O when the Mg/Al molar ratio is 3.0 indicates that magnesium atoms incline to attract more surrounding atoms especially oxygen. This result is due to the fact that the binding arrangement between Mg^{2+} and O^{2-} is also highest at the same ratio. It can be concluded that the CO_2 capture capacity of amorphous LDOs is closely related to the Mg/Al molar ratio due to the high value of g*(r).

4) This study describes a promising simulation method to investigate the characteristics of LDH and LDH-derived amorphous LDO and the results provide molecular-scale insight into the structural and dynamical origins of the interactions of CO_2 with LDO. This can be helpful to design LDO structures with optimal CO_2 capture capacities.

5.2 Future works

Due to the limited computational resource, current molecular dynamics simulations were conducted with 3D periodic conditions. The regeneration process of the structure of the calcined LDH occur via intercalation of hydroxyl groups after contact with anions solution [74]. However, the LDH-derived mixed oxide did not recover their original layered structure in MD simulation. With the development of MD technique and computer science, the memory effect of LDH shall be included in the future study.

Furthermore, the CO_2 chemisorption on single-layer aluminum nitride nanostructures is kinetically and thermodynamically accessible at room temperature due to the low energy barrier between physisorption and chemisorption [75]. In addition, the bonding interactions are formed between C-N and O-Al in the chemisorption structure, which contribute to CO_2 adsorption capacity. However, only the CO_2 physisorption of amorphous LDO is considered in current study. Thus, the CO_2 chemisorption of amorphous LDO in MD simulation is necessary to investigate.

References

[1] J. D. Figueroa, T. Fout, S. Plasynski, H. McIlvried, and R. D. Srivastava, "Advances in CO_2 capture technology-The U.S. Department of Energy's Carbon Sequestration Program," *Int. J. Greenh. Gas Control*., vol. 2, no. 1, pp. 9–20, 2008.

[2] H. H. Kehrer, "Fossil Fuel Combustion and the Major sediment cycle," *Science*., vol. 173, no. July, pp. 233–235, 1971.

[3] Z. Yong, V. Mata, and E. Rodrigues, "Adsorption of Carbon Dioxide onto Hydrotalcite-like Compounds (HTlcs) at High Temperatures," *Ind. Eng. Chem. Res.*, vol. 40, no. 1, pp. 204–209, 2001.

[4] T. Searchinger *et al.*, "Emissions from Land-Use Change," *Science*., vol. 423, no. February, pp. 1238–1241, 2008.

[5] H. Yang *et al.*, "Progress in carbon dioxide separation and capture: A review," *J. Environ. Sci.*, vol. 20, no. 1, pp. 14–27, 2008.

[6] M. Kanniche, R. Gros-Bonnivard, P. Jaud, J. Valle-Marcos, J. M. Amann, and C. Bouallou, "Pre-combustion, post-combustion and oxy-combustion in thermal power plant for CO_2 capture," *Appl. Therm. Eng.*, vol. 30, no. 1, pp. 53–62, 2010.

[7] J. Hufton, S. J. Weigel, S. Nataraj, M. Rao, and S. Sircar, "Proceedings of the 1999 U.S DOE Hydrogen Program Review NREL/CP-570-26938," *Proc. 1999 U.S DOE Hydrog. Progr. Rev.*, 1999.

[8] X. Xu, J. M. Andrésen, C. Song, B. G. Miller, and A. W. Scaroni, "Novel adsorbent for CO_2 capture based on polymer-modified mesoporous molecular sieve of MCM-41 type," no. 18, pp. 1463–1469, 2002.

[9] G. R. Williams and D. O'Hare, "Towards understanding, control and application of layered double hydroxide chemistry," *J. Mater. Chem.*, vol. 16, no. 30, p. 3065, 2006.

[10] V. Rives and S. Kannan, "Layered double hydroxides with the hydrotalcite-type structure containing Cu^{2+}, Ni^{2+} and Al^{3+}," *J. Mater. Chem.*, vol. 10, no. 2, pp. 489–495, 2000.

[11] Y. Ding and E. Alpay, "High Temperature Recovery of CO_2 from Flue Gases Using Hydrotalcite Adsorbent," *Process Saf. Environ. Prot.*, vol. 79, no. 1, pp. 45–51, 2001.

[12] J. Blamey, E. J. Anthony, J. Wang, and P. S. Fennell, "The calcium looping cycle for large-scale CO_2 capture," *Prog. Energy Combust. Sci.*, vol. 36, no. 2, pp. 260–279, 2010.

[13] M. Alonso, N. Rodríguez, B. González, B. Arias, and J. C. Abanades, "Biomass Combustion with in Situ CO_2 Capture by CaO. II. Experimental Results," *Ind. Eng. Chem. Res.*, vol. 50, no. 11, pp. 6982–6989, 2011.

[14] J. R. Fernández, J. C. Abanades, R. Murillo, and G. Grasa, "Conceptual design of a hydrogen production process from natural gas with CO_2 capture using a Ca-Cu chemical loop," *Int. J. Greenh. Gas Control*, vol. 6, pp. 126–141, 2012.

[15] I. Martínez, G. Grasa, R. Murillo, B. Arias, and J. C. Abanades, "Kinetics of calcination of partially carbonated particles in a Ca-looping system for CO_2 capture," *Energy and Fuels*, vol. 26, no. 2, pp. 1432–1440, 2012.

[16] Karunasena, Gi and Amaratunga, International conference on sustainable built environment 2010.

[17] F. Cavani, F. Trifirò, and A. Vaccari, "Hydrotalcite-type anionic clays: Preparation, properties and applications.," *Catal. Today*, vol. 11, no. 2, pp. 173–301, 1991.

[18] S. P. Newman and W. Jones, "Synthesis, characterization and applications of layered double hydroxides containing organic guests," *New J. Chem.*, vol. 22, pp. 105–115, 1998.

[19] N. D. Hutson, S. a. Speakman, and E. A. Payzant, "Structural Effects on the High Temperature Adsorption of CO_2 on a Synthetic Hydrotalcite," *Chem. Mater.*, vol. 16, no. 21, pp. 4135–4143, 2004.

[20] W. Yang, Y. Kim, P. K. T. Liu, M. Sahimi, and T. T. Tsotsis, "A study by in situ techniques of the thermal evolution of the structure of a Mg–Al–CO_3 layered double hydroxide," *Chem. Eng. Sci.*, vol. 57, no. 15, pp. 2945–2953, 2002.

[21] T. Hibino and A. Tsunashima, "Characterization of repeatedly reconstructed Mg-Al hydrotalcite-like compounds: gradual segregation of aluminum from the structure," *Chem. Mater.*, no. 20, pp. 4055–4061, 1998.

[22] V. Borau, M. Luque, M. Marinas, Y. Avile, R. Ruiz, and F. J. Urbano, "Hydroxides : a Spectroscopic Study," , *J. Mater. Chem.*, pp. 2–6, 2000.

[23] S. Choi, J. H. Drese, and C. W. Jones, "Adsorbent materials for carbon dioxide capture from large anthropogenic point sources," *ChemSusChem*, vol. 2, no. 9, pp. 796–854, 2009.

[24] Q. Wang *et al.*, "The effect of trivalent cations on the performance of Mg-M-CO_3 layered double hydroxides for high-temperature CO_2 capture," *ChemSusChem*, vol. 3, no. 8, pp. 965–973, 2010.

[25] M. K. R. Reddy, Z. P. Xu, G. Q. M. Lu, and J. C. D. Costa, "Layered Double Hydroxides for CO_2 Capture : Structure Evolution and Regeneration," *Society*, vol. 45, no. 22, pp. 7504–7509, 2006.

[26] Y. Gao *et al.*, "Comprehensive investigation of CO_2 adsorption on Mg–Al–CO_3 LDH-derived mixed metal oxides," *J. Mater. Chem. A*, vol. 1, no. 41, pp. 12782–12790, 2013.

[27] U. Sharma, B. Tyagi, and R. Jasra, "Synthesis and Characterization of Mg−Al−CO_3 Layered Double Hydroxide for CO_2 Adsorption," *Ind. Eng. Chem.*, pp. 9588–9595, 2008.

[28] M. León, E. Díaz, S. Bennici, A. Vega, S. Ordóñez, and A. Auroux, "Adsorption of CO_2 on hydrotalcite-derived mixed oxides: Sorption mechanisms and consequences for adsorption irreversibility," *Ind. Eng. Chem. Res.*, vol. 49, no. 8, pp. 3663–3671, 2010.

[29] N. N. A. H. Meis, J. H. Bitter, and K. P. D. Jong, "Support and size effects of activated hydrotalcites for precombustion CO_2 capture," *Ind. Eng. Chem. Res.*, vol. 49, no. 3, pp. 1229–1235, 2010.

[30] M. Bolognini, F. Cavani, D. Scagliarini, C. Flego, C. Perego, and M. Saba, "Heterogeneous basic catalysts as alternatives to homogeneous catalysts: Reactivity of Mg/Al mixed oxides in the alkylation of m-cresol with methanol," *Catal. Today*, vol. 75, no. 1–4, pp. 103–111, 2002.

[31] Belloto Maurizio, R. Bernadette, C. Olivier, L. John, B. Dominique, and E. Elkaim, "A Reexamination of Hydrotalcite Chemistry," *J. Phys. Chem.*, vol. 100, no. 20, pp. 8527–8534, 1996.

[32] P. P. Kumar, A. G. Kalinichev, and R. J. Kirkpatrick, "Molecular dynamics simulation of the energetics and structure of layered double hydroxides intercalated with carboxylic acids," *J. Phys. Chem. C*, vol. 111, no. 36, pp. 13517–13523, 2007.

[33] P. P. Kumar, A. G. Kalinichev, and R. J. Kirkpatrick, "Hydration, swelling, interlayer structure, and hydrogen bonding in organolayered double hydroxides: Insights from molecular dynamics simulation of citrate-intercalated hydrotalcite," *J. Phys. Chem. B*, vol. 110, no. 9, pp. 3841–3844, 2006.

[34] A. G. Kalinichev, P. Padma Kumar, and R. James Kirkpatrick, "Molecular dynamics computer simulations of the effects of hydrogen bonding on the properties of layered double hydroxides intercalated with organic acids," *Philos. Mag.*, vol. 90, no. June, pp. 2475–2488, 2010.

[35] Q. Zhao and S. E. Burns, "Molecular dynamics simulation of secondary sorption behavior of montmorillonite modified by single chain quaternary

ammonium cations," *Environ. Sci. Technol.*, vol. 46, no. 7, pp. 3999–4007, 2012.

[36] R. T. Cygan, J.-J. Liang, and A. G. Kalinichev, "Molecular Models of Hydroxide, Oxyhydroxide, and Clay Phases and the Development of a General Force Field," *J. Phys. Chem. B*, vol. 108, no. 4, pp. 1255–1266, 2004.

[37] E. by B. Pullman, *Intermolecular Forces*. 1981.

[38] B. J. Teppen, K. Rasmussen, P. M. Bertsch, D. M. Miller, and L. Schäfer, "Molecular Dynamics Modeling of Clay Minerals. 1. Gibbsite, Kaolinite, Pyrophyllite, and Beidellite," *J. Phys. Chem. B*, vol. 101, no. 9, pp. 1579–1587, 1997.

[39] J. R. HILL and J. SAUER, "Molecular mechanics potential for silica and zeolite catalysts based on ab initio calculations. 2. Aluminosilicates," *J. Phys. Chem.*, vol. 99, no. 23, pp. 9536–9550, 1995.

[40] P. Dauber-Osguthorpe, V. A. Roberts, D. J. Osguthorpe, J. Wolff, M. Genest, and A. T. Hagler, "Structure and energetics of ligand binding to proteins: Escherichia coli dihydrofolate reductase-trimethoprim, a drug-receptor system.," *Proteins*, vol. 4, no. 1, pp. 31–47, 1988.

[41] V. A. Ermoshin, K. S. Smirnov, and D. Bougeard, "Ab initio generalized valence force field for zeolite modeling. 2. Aluminosilicates," *Chem. Phys.*, vol. 209, pp. 41–51, 1996.

[42] V. A. Ermoshin, K. S. Smirnov, and D. Bougeard, "Molecular dynamics calculation of the vibrational spectra of OH groups in zeolites and on silica surfaces," *Surf. Sci.*, vol. 368, no. 1–3, pp. 147–151, 1996.

[43] D. Bougeard, K. S. Smirnov, and E. Geidel, "Vibrational Spectra and Structure of Kaolinite : A Computer Simulation Study," pp. 9210–9217, 2000.

[44] C. I. Sainz-Diaz, A. Hernández-Laguna, and M. T. Dove, "Modeling of diotahedral 2:1 phyllosilicates by means of transferable empirical potentials," *Phys. Chem. Miner.*, vol. 28, no. 2, pp. 130–141, 2001.

[45] R. T. Cygan, J. a. Greathouse, H. Heinz, and A. G. Kalinichev, "Molecular models and simulations of layered materials," *J. Mater. Chem.*, vol. 19, no. 17, p. 2470, 2009.

[46] M. Thyveetil, P. Coveney, H. Greenwell, and J. Suter, "Computer simulation study of the structural stability and materials properties of DNA-intercalated layered double hydroxides," *J. Am. Chem. Soc.*, no. 8, pp. 4742–4756, 2008.

[47] A. Zhu, X. Zhang, Q. Liu, and Q. Zhang, "A Fully Flexible Potential Model for Carbon Dioxide," *Chinese J. Chem. Eng.*, vol. 17, no. 2, pp. 268–272, 2009.

[48] R. T. Cygan, V. N. Romanov, and E. M. Myshakin, “Molecular simulation of carbon dioxide capture by montmorillonite using an accurate and flexible force field,” *J. Phys. Chem. C*, vol. 116, no. 24, pp. 13079–13091, 2012.

[49] C. L. Kong, “Combining rules for intermolecular potential parameters. II. Rules for the Lennard-Jones (12–6) potential and the Morse potential,” *J. Chem. Phys.*, vol. 59, no. 5, pp. 2464–2467, 1973.

[50] H. J. S. Feder and J. J. E. Slotine, “Real-time path planning using harmonic potentials in dynamic environments,” *Int. Conf.*, vol. 1, no. 4, pp. 874–881, 1997.

[51] M. Parrinello and A. Rahman, “Polymorphic transitions in single crystals: A new molecular dynamics method,” *J. Appl. Phys.*, vol. 52, no. 12, pp. 7182–7190, 1981.

[52] S. Nosé, “A unified formulation of the constant temperature molecular dynamics methods,” *J. Chem. Phys.*, 1984.

[53] W. G. Hoover, “Canonical dynamics: Equilibrium phase-space distributions,” *Phys. Rev. A*, vol. 31, no. 3, pp. 1695–1697, 1985.

[54] G. Gutierrez, a B. Belonoshko, R. Ahuja, and B. Johansson, “Structural properties of liquid Al_2O_3: A molecular dynamics study,” *Phys. Rev. E*, vol. 61, no. 3, pp. 2723–2729, 2000.

[55] D.-Y. Peng and D. B. Robinson, “A New Two-Constant Equation of State,” *Ind. Eng. Chem. Fundam.*, vol. 15, no. 1, pp. 59–64, 1976.

[56] S. Plimpton, “Fast Parallel Algorithms for Short-Range Molecular Dynamics,” *Journal of Computational Physics*., vol. 117, no. 1. pp. 1–19, 1995.

[57] C. Rycroft, “Voro++: A three-dimensional Voronoi cell library in {C++},” *Lawrence Berkeley Natl. Lab.*, pp. 1–14, 2009.

[58] A. Stukowski, “Visualization and analysis of atomistic simulation data with OVITO–the Open Visualization Tool,” *Model. Simul. Mater. Sci. Eng.*, vol. 18, no. 1, p. 15012, 2009.

[59] J. R. Maple *et al.*, “Derivation of class II force fields. I. Methodology and quantum force field for the alkyl functional group and alkane molecules,” *J. Comput. Chem.*, vol. 15, no. 2, pp. 162–182, 1994.

[60] P. D’Arco, M. Causà, C. Roetti, and B. Silvi, “Periodic Hartree-Fock study of a weakly bonded layer structure: Brucite $Mg(OH)_2$,” *Phys. Rev. B*, vol. 47, no. 7, pp. 3522–3529, 1993.

[61] H. Nakayama, N. Wada, and M. Tsuhako, “Intercalation of amino acids and peptides into Mg-Al layered double hydroxide by reconstruction method,” *Int. J. Pharm.*, vol. 269, no. 2, pp. 469–478, 2004.

[62] S. Miyata, “Physico-Chemical Properties of Synthetic Hydrotalcites in Relation to Composition,” *Clays Clay Miner.*, vol. 28, no. 1, pp. 50–56, 1980.

[63] Y. Belmabkhout, R. Serna-Guerrero, and A. Sayari, “Adsorption of CO_2 from dry gases on MCM-41 silica at ambient temperature and high pressure. 1: Pure CO_2 adsorption,” *Chem. Eng. Sci.*, vol. 64, no. 17, pp. 3721–3728, 2009.

[64] M. Khalkhali, “CO_2 capture capacity of hydrotalcite-derived oxides : An atomistic simulation study Department of Chemical and Materials Engineering , University of Alberta, Edmonton, T6G 1H9, Canada, and Key Laboratory for Thermal Science and Power Engineering of M,” pp. 1–33.

[65] B. G. Levine, J. E. Stone, and A. Kohlmeyer, “Fast analysis of molecular dynamics trajectories with graphics processing units — Radial distribution function histogramming,” *J. Comput. Phys.*, vol. 230, no. 9, pp. 3556–3569, 2011.

[66] R. W. Impey, P. A. Madden, and I. R. McDonald, “Hydration and Mobility of Ions in Solution,” *J. Phys. Chem.*, vol. 87, no. 25, pp. 5071–5083, 1983.

[67] M. Khalkhali, H. Zeng, Q. Liu, and H. Zhang, “Structural Evolutions of ZnS Nanoparticles in Hydrated and Bare States,” *J. Phys. Chem. C*, vol. 120, no. 14, pp. 7870–7884, 2016.

[68] B. Cichocki and K. Hinsen, “Dynamic computer simulation of concentrated hard sphere suspensions. I. Simulation technique and mean square displacement data,” *Phys. A Stat. Mech. its Appl.*, vol. 166, no. 3, pp. 473–491, 1990.

[69] P. G. Shewmon, “Surface diffusion from a point source,” *J. Appl. Phys.*, vol. 34, no. 4, pp. 755–757, 1963.

[70] A. B. Shelekhin, A. G. Dixon, and Y. H. Ma, “Theory of gas diffusion and permeation in inorganic molecular sieve membranes,” *AIChE J.*, vol. 41, no. 1, pp. 58–67, 1995.

[71] H. Yucel and D. M. Ruthven, “Diffusion of CO_2 in 4A and 5A zeolite crystals,” *J. Colloid Interface Sci.*, vol. 74, no. 1, pp. 186–195, 1980.

[72] B. Jähne, G. Heinz, and W. Dietrich, “Measurement of the diffusion coefficients of sparingly soluble gases in water,” *J. Geophys. Res. Ocean.*, vol. 92, no. C10, pp. 10767–10776, 1987.

[73] Z. Yong and A. E. Rodrigues, “Hydrotalcite-like compounds as adsorbents for carbon dioxide,” *Energy Convers. Manag.*, vol. 43, no. 14, pp. 1865–1876, 2002.

[74] L. P. Cardoso and J. B. Valim, “Study of acids herbicides removal by calcined Mg-Al-CO_3-LDH,” *J. Phys. Chem. Solids*, vol. 67, no. 5–6, pp. 987–993, 2006.

[75] Y. Jiao et al., "Adsorption of Carbon Dioxide and Nitrogen on Single-Layer Aluminum Nitride Nanostructures Studied by Density Functional Theory," *J. Phys. Chem. C,* vol. 114, pp. 7846-7849, 2010.